Reducing CO2 Flow Using Foams

Guillaume Batot, Marc Fleury, Lahcen Nabzar

Available online at www.sciencedirect.com

ScienceDirect

Energy Procedia 114 (2017) 4129 – 4139

Energy Procedia

13th International Conference on Greenhouse Gas Control Technologies, GHGT-13, 14-18 November 2016, Lausanne, Switzerland

Reducing CO_2 flow using foams

Guillaume Batôt*, Marc Fleury, Lahcen Nabzar

IFP Energies nouvelles, 1 avenue de Bois-Préau, 92852 Rueil-Malmaison, France

Abstract

As part of the MiReCOL three-year European project (www.mirecol-co2.eu) on storage remediation technologies, we studied in the laboratory the capacity of foams to reduce gas flow for CO_2-brine systems in rock core sample with common surfactants, as a function of interstitial velocity and gas to water fraction. Two different types of experimental set-up are used. They both allow local measurement of the water saturation for low and high pressure/temperature condition. A small MRI core-flood set-up is used to perform experiments at 35°C and 10 bars pore pressure, in CO_2 non-dense condition. In order to work under reservoir condition, at 40°C and 130 bars, with dense super-critical CO_2 we used a classical core-flood system coupled to an X-ray detection set-up.

All experiments were carried out in similar Clashach sandstones with permeability between 220 and 1500 mD, and porosity in the range 10-20%. The gas and the surfactant-brine solution were co-injected at the core inlet face with a gas fraction around 0.7. We vary the interstitial velocity within two decades from about 3 ft/day up to 100 ft/day.

The performance of the generated foams was evaluated from the relative foam viscosity, the ratio of the measured pressure drop in the presence of foam to the pressure drop in single phase condition for the same interstitial velocity. Whatever the pressure and permeability/porosity, the relative foam viscosity can be described as a power law vs. the shear rate evaluated from the interstitial velocity, permeability and porosity. The exponent is close to -1 describing the shear-thinning behavior.

Peer-review under responsibility of the organizing committee of GHGT-13.

Keywords: remediation, foam, CO2, shear thinning, effective viscosity

* Corresponding author. *Email-address* : guillaume.batot@ifpen.fr

Peer-review under responsibility of the organizing committee of GHGT-13.
doi:10.1016/j.egypro.2017.03.1553

1. Introduction

The oil and gas industry has a long-term experience in reducing the flow rate of a given fluid, or maximizing the oil and gas recovery, by injecting fluids with specific properties into rock formations containing hydrocarbons. As it has already been stated[1], Carbon Capture and Sequestration programs (CCS) could benefit from the CO_2-Enhanced-Oil-Recovery knowledge. Indeed, in the EOR context, the gas-based injections are now the most common methods since the decline of the thermal ones in the early 2000's [2]. Due to its unique properties such as low minimum miscibility pressure, CO_2 has been mainly used in such techniques.

Beyond their use for mobility control in EOR, foams can also be adequate to secure gas storage operations through gas confinement and leakage prevention/remediation. Regarding CO_2 storage operations, gas confinement is of great importance to ensure that such process can be used as a safe and effective solution for greenhouse mitigation. A clear insight on the associated risks, their sound evaluation and the development of means for their prevention and mitigation are thus needed. Risks of CO_2 leakage through/along wells, faults and fractures and through the sealing cap-rock are among the most important. Indeed, due to its low density and high mobility, gas might potentially migrate out of the storage zone towards the upper formation due to gravity segregation and finally might leak into the atmosphere. This leakage potential is mainly determined around the well and on the sealing cap rock integrity. Due to their ability to preferentially restrict fluid flow in the most permeable areas, foams are particularly indicated to address the leakage from high permeability areas or through fracture and fissures that are considered as the most important leakage pathways [3].

The foam lifetime in the porous media may be about few weeks, at best, thus the use of classical foams in a CCS context is adapt for emergency remediation but for mid-term prevention gel-foam [4] can be designed. For both, classical and gel foams, laboratory experiments in rock samples are based on the evaluation of the gas flow resistance of the foam lamellae. The gel-foam implies a complementary chemical study on the relevant cross-linkers needed to gel the foam. In the following we focus only on the foam generation, propagation, and its ability to reduce the gas flow rate in porous media.

2. Foam generation and propagation in porous media

Despite numerous theoretical studies [5,6], experimental works [4,7,8] and field/pilot tests [9–11] dedicated to foam processes, it is still a developing technology and uncertainties remains regarding the governing parameters of this complex physics. On several aspects, foams generated in rock formations are very different from the "everyday life" or "bulk" foam that we are familiar with. In porous media they can be seen as finely-textured gas bubbles, such as nitrogen, methane or carbon dioxide, dispersed within brine. Their formation requires a certain amount of energy, which is provided by shearing along the porous structure, and are stabilized by surfactants that are generally solubilized in the water, but could also be dissolved into the CO_2 [12,13]. The gas bubbles are separated by liquid films called lamellae, responsible for the reduction of the gas flow. In homogeneous structure, lamellae creation results from two main identified mechanisms [5]: the lamellae division and the gas bubble snap-off. A third mechanism is also identified, the leave-behind, but it can be seen as a specific case of the lamellae division. Thus, the gas transport properties may result from a dynamic equilibrium between lamellae creation and destruction.

At the laboratory scale, the resistance to gas flow, *i.e.* the resistance of the lamellae to coalescence, is evaluated macroscopically within rock core sample from the pressure drop ΔP_{foam} along the core. The so-called gas Mobility Reduction Factor (MRF) is defined as the following ratio $\Delta P_{\text{foam}}/\Delta P_{\text{ref}}$, which can be seen as a relative and apparent viscosity of the generated foam at a given flow rate. The reference pressure drop can be the water pressure drop (monophasic reference) or the pressure drop measured from a water and gas co-injection (diphasic reference).

In the absence of oil, the lamellae coalescence seems to be mainly governed by the capillary pressure P_c and the local water saturation S_w. Two regimes of foam flow have been distinguished [8] : in the P_c^* regime, when the P_c is close, or equal, to the limiting value P_c^*, the generated foam is "strong" and provides high MRF; below the P_c^* the foam is "weak" and does not give large resistance to gas flow. At a given total flow rate, the capillary pressure can be increased with the gas fractional flow, or foam quality, denoted as $f_g = \frac{Q_g}{Q_w+Q_g}$ the gas flow rate divided by the total flow rate. When the limiting capillary pressure P_c^* is reached, further increase in the foam quality induces instabilities through coarsening of the foam texture. There is an upper limit, mostly over f_g~0.9, above which foam collapses due to "dry out" effect.

In the P_c^* regime two flow regimes exist and the transition occurs at a critical or optimal gas fraction f_g^* corresponding to the critical capillary pressure and to the maximum in pressure drop at a given total flow rate. With low quality wet foam, $f_g < f_g^*$, the pressure drop is almost independent of the liquid flow rate while for dry foam at high quality, $f_g > f_g^*$ it becomes almost independent of the gas flow rate [14]. The optimal foam quality is usually obtained between 0.7 and 0.9 [15]. Thus, according to this view, the foam-induced pressure drop usually exhibits a maximum when plotted against foam quality [15–18]. This maximum is reached at the optimal foam quality f_g^* that depends on system characteristics and especially on formation permeability, surfactant and flow rate. This optimal foam quality is a very important parameter to determine for a given application case.

It has been demonstrated that for strong foam generation, a minimum pressure gradient or a minimum critical velocity is required [4]. Once these strong foams are generated, inside the porous media, their rheological behavior shows the following main trends: first, MRF increases with increasing velocity up to a maximum. Then MRF decreases when increasing further the velocity beyond the maximum (shear thinning behavior). Finally, MRF shows hysteresis effect when the velocity is decreased. Such typical rheological behavior is illustrated on Figure 1.

Most of the foams exhibit the shear thinning behavior. This is an important advantage for the use of foams in EOR for sweep improvement. Indeed, foams are usually generated in situ in the near wellbore area where the velocity is high leading to low MRF that mitigate the injectivity issue. Far away from wellbore, the velocity decreases leading to higher MRF with better gas blocking performance.

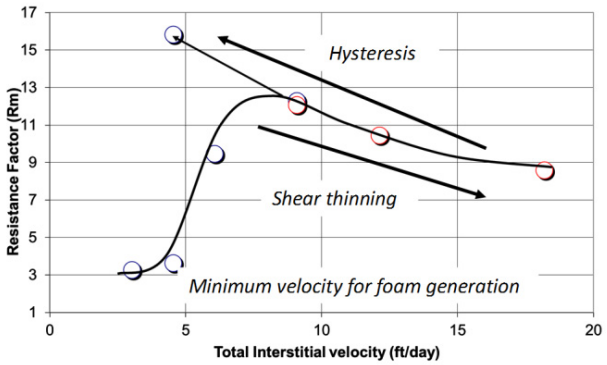

Figure 1: Typical behavior of foam when increasing the total interstitial velocity. Hysteresis may occur with decreasing velocity, yielding higher resistance to gas far from the well (Nabzar, 2014, ADRAC, Abu Dhabi). Conditions: 40°C, 130 bar.

3. Materials and methods

Experiments presented in this work were carried out in Clashach sandstones with a water permeability between 225

mD and 1550 mD and a porosity between 10% and 20%. Depending on the experimental set-up, two different plug sizes are used, the smallest ones have a pore volume of 1.5 and 2.5 ml with a length of 4.0 cm and a radius of 1.0 cm, while the largest has a pore volume of 25 ml with a length of 10.0 cm and a radius of 2.0 cm. The water used is a 3.5wt% NaCl brine. Surfactant is a classical AOS type (Rhodacal® A-246/L manufactured by Solvay) prepared at the concentration of 0.5 wt. % in this brine.

A typical experiment consists in first co-injecting brine and pure CO_2, and then brine is replaced by a solution of the same brine but containing a surfactant. In all these experiments CO_2 and surfactant-brine are co-injected at the core inlet to make sure that the foam is generated by shearing through the porous structure, and not before. The foam quality f_g, or gas fraction, is fixed around 0.7. Various total flow rates varying from near wellbore to in depth fluid velocities can be explored in an experiment.

3.1. MRI system at low pressure

With the MRI small core-flood set-up (Figure 2), brine and pure CO_2 are co-injected at the top inlet face of the sample. The flooding cell is custom built and specifically designed for MRI systems: sample diameter is 2.0 cm with a maximum sample length of 5.0 cm; NMR probe diameter is 3.0 cm; the maximum confining pressure is 80 bar and 10 bar pore pressure is imposed by a membrane back-pressure regulator (BPR); the temperature is fixed around 30°C (MRI magnet temperature). The liquid and gas flow rates are respectively imposed using a pump (QX-6000 from Quizix) and a gas controller (EL-Flow® from Bronkhorst®). We vary the total flow rate Q_t by a factor of 100, from 1 cm^3/h up to 100 cm^3/h, corresponding in this case to interstitial velocity $v_i = Q_t/(S\phi)$ between 1.6 and 160 cm/h, or between 1.22 and 122 ft/day in usual engineering units. During injection, we continuously measure by standard MRI techniques the saturation profiles (a spin echo sequence) and the T_2 relaxation time distributions typically every minute.

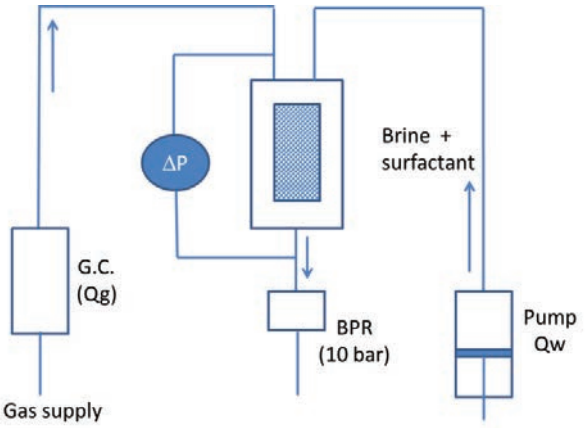

Figure 2: Schematic of the experimental set-up using NMR imaging. Gas controller (G.C.) to impose a fixed gas flow rate. Back pressure regulator (BPR): used to set the outlet pressure. The MRI system is a 20 MHz compact permanent magnet system from Oxford Instrument.

3.2. X-Ray system at high pressure

The high pressure system is conceptually similar and is composed of a horizontal composite core holder with low X-ray attenuation. The X-ray generator (90keV – Ta filter) and the detector can move along the heated Hassler cell using a step by step motor. A full-length scan every 5 mm takes about 15 min. A saturation profile is calculated from the measured X-ray profile and two calibration profiles (sample fully saturated with brine and dry). The CO_2 is injected from a high pressure piston-cylinder cell at the chosen working pressure and temperature; experiments were carried out at 40°C and 130 bar pore pressure with 180 bar of overburden pressure; the core sample used had a water permeability of 820 mD and a porosity of 20.2 %. The total flow rate was changed from 10 to 300 cm^3/h yielding

interstitial velocities between 3.9 and 119.3 cm/h (3.1 and 94.0 ft/day) in the same range as in the MRI setup. At 40°C and 130 bars, the injected CO_2 is in a supercritical dense state with a density of 743 ± 3.7 kg/m^3 (from NIST database).

4. Results

4.1. Low pressure system: transient regime before foam formation

Here we focus on the onset of foam at the lowest flow rate (1 cm^3/h or 1.6cm/h, Figure 3). The sample is a Clashach sandstone of porosity 20.2% and water permeability 1550 mD. The sample was used for several foam experiments before this one and therefore adsorption of the surfactant on the solid surface is stabilized. A foam generating a strong pressure drop is only observed when the water saturation is low enough (~15%), corresponding to high capillary pressure close to irreducible water saturation (Figure 3 - left). This is achieved after a few pore volume (PV). Then, at a nearly constant water saturation and during a few pore volume also, a strong foam is abruptly formed as indicated by the sharp increase of the pressure drop after injection of 2 PV or at this low flow rate after t= 6.2 hr. Interestingly, the saturation profiles (Figure 3 - right) are nearly uniform for strong foams and this uniform profile is gradually achieved starting from the middle of the sample.

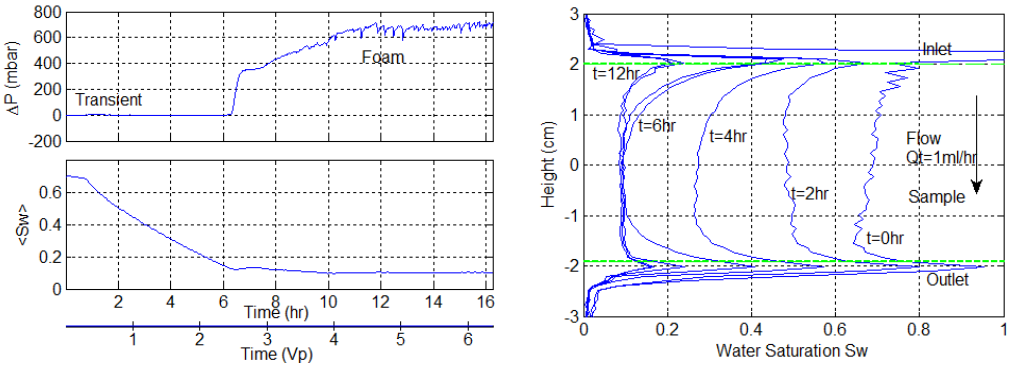

Figure 3: [Left] Generation of foam at a low interstitial velocity (1 ml/h, 1.6 cm/h) : Clashach sandstone, porosity 20.2%, 1550 mD, f_g=0.6, brine 35 g/l, AOS type surfactant concentration 0.5 wt%.[Right] Local saturation profiles corresponding to the left graph every 2 hours. At t=6 hr, a strong foam is present. The spikes at the inlet and outlet correspond to the liquid present in the injectors. The average saturation is calculated with the values between the green horizontal lines.

4.2. Low pressure system: foam apparent viscosity

At steady state, the mobility reduction factor is calculated as the ratio of the measured pressure drop in the presence of foam $\Delta P_{foam}(Q_t; f_g \sim 0.7)$ to the one during a single phase brine injection $\Delta P_{brine}(Q_t)$ at the same total flow rate Q_t:

$$MRF(Q_t; f_g) = \frac{\Delta P_{foam}(Q_t; f_g \sim 0.7)}{\Delta P_{brine}(Q_t)}. \quad (1)$$

Indeed, as shown by 3D CT-scan imaging [7], defining the mobility reduction factor with the pressure drop in two phase flow conditions (co-injection of gas and brine without surfactants) in such short samples has little meaning due to severe digitation problems. Based on the Darcy law, with this definition the MRF can be seen as the foam relative apparent viscosity, denoted as η_r^f in the following, which corresponds to the ratio of the foam apparent viscosity to the brine viscosity $\eta_{app}^f / \eta_{brine}$.

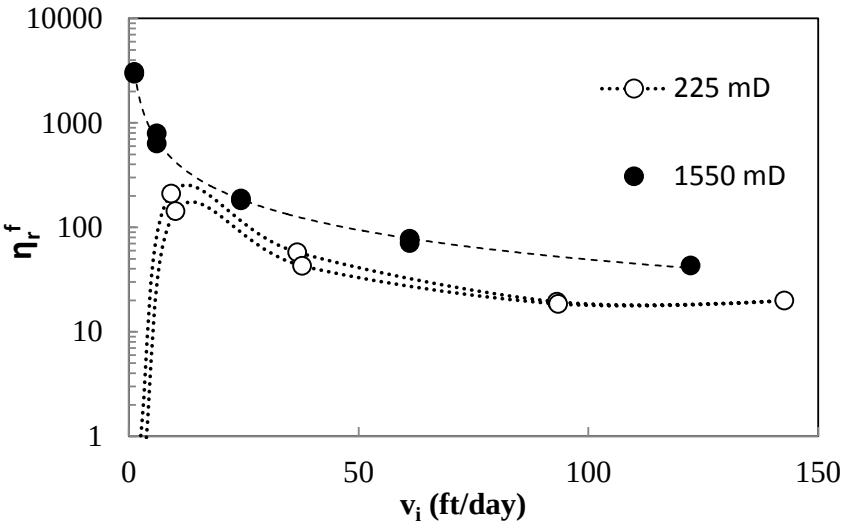

Figure 4: Foam relative viscosity in a small core of Clashach sandstone plotted against the interstitial velocity. Full circles correspond to the date obtain with a core of 1550 mD water permeability and 20.2% of porosity. Empty circles are the data for 225 mD and 12.1% porosity. Points are obtained with both increasing and decreasing velocities (duplicate points).

On Figure 4 the foam relative viscosity η_r^f is plotted against the total interstitial velocity for the two permeability values. The data obtained from increasing and decreasing total flow rate are very similar (duplicate points). In the less permeable rock sample, at the lowest interstitial velocity of 2.2 ft/day, the measured apparent viscosity is very close to 1, suggesting that there is strictly speaking no foam generated at this point. At 9.2 ft/day we observed a rise of the pressure drop and strong water desaturation of the porous media, leading to a relative viscosity about 100-200. No such critical velocity is observed with the more permeable core, as it may be too small to be measured with the present experimental set-up.

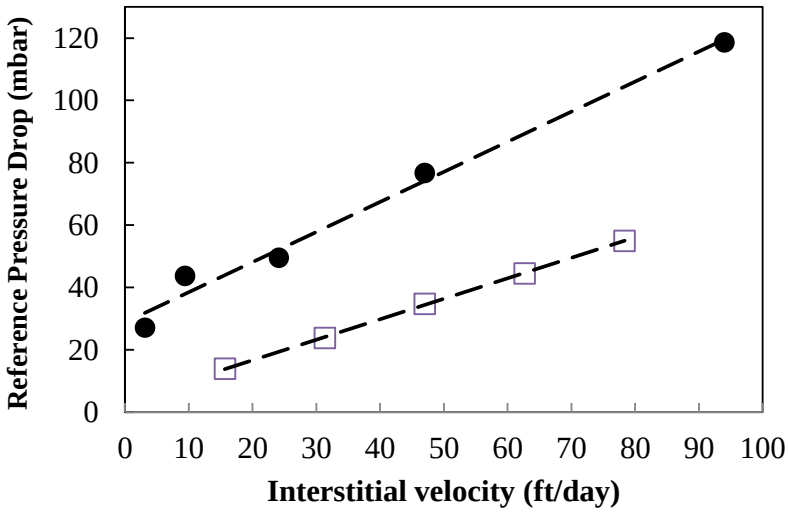

Figure 5: Pressure drops for several interstitial velocities. Empty squares are the measurements from the injection of water without surfactants, while the full circle from the co-injection of gas and water still without surfactants. Dotted lines are linear regressions.

4.3. High pressure system: foam apparent viscosity

The flooding cell used with the high pressure setup allows working with longer core sample. With the 10 cm length plug a reference pressure drops measurement from CO_2 and water co-injection can be performed without any surfactant (Figure 5). The data are well described by linear relationships and both linear regressions can be used to evaluate either the performance ratio between foam and gas/water co-injection MRF $= \Delta P_{\text{foam}}/\Delta P_{\text{water-gas}}$, or the relative foam viscosity $\Delta P_{\text{foam}}/\Delta P_{\text{water}}$.

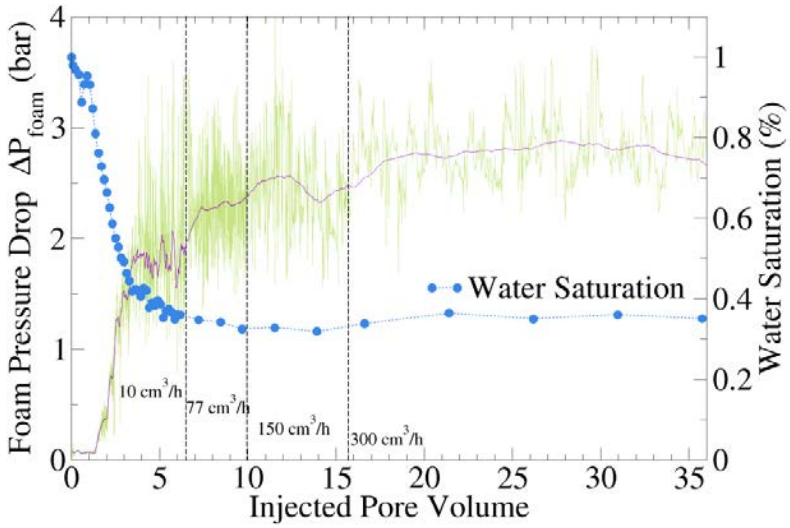

Figure 6: Dense supercritical CO_2-foam generation in a 820 mD Clashach sandstone. The line in dark purple is a running average of 200 points of the raw pressure drop measurement represented here in light green. The full circles represent the mean water saturation along the core. Data are plotted against the total injected pore volume and thus not linear in time as the total flow rate was increased from 10 up to 300 cm^3/h.

During the foam generation and propagation in the porous media, the mean water saturation is recorded from X-ray absorbance technique. During the first four injected pore volumes, at the total flow rate of 10 cm^3/h (or 3.1 ft/day interstitial velocity), the transient regime of the initial foam formation is clearly observed and correlated to a fast water desaturation (Figure 6). Increasing the total flow rate increases the pressure drop as expected if the foam still exist and does not coalesce. The MRF evolution evaluated from the diphasic co-injection of water and gas (Figure 7) is typical of a shear thinning mechanism.

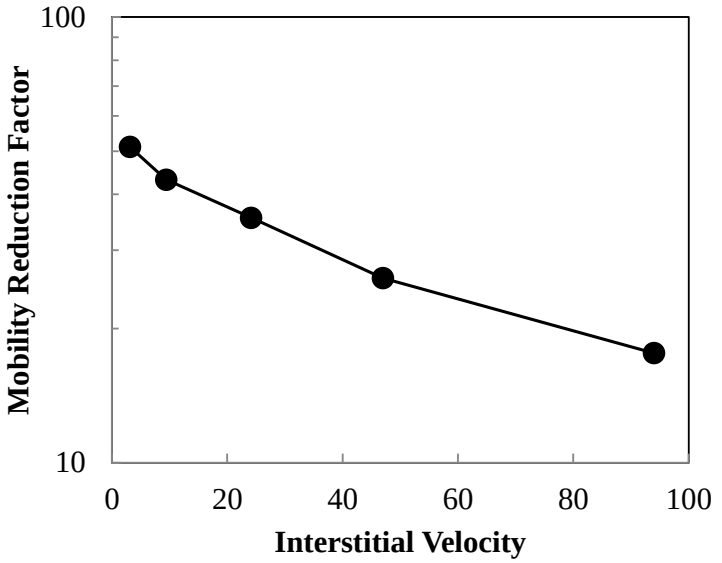

Figure 7: Mobility Reduction Factor evaluated from the performance ratio between foam and gas/water co-injection MRF = $\Delta P_{\text{foam}}/\Delta P_{\text{water-gas}}$. The $\Delta P_{\text{water-gas}}$ is extracted from the linear regression of raw data (Figure 5).

5. Synthesis

As the interstitial velocity takes into account the porosity, it is not an adequate variable to compare results between plugs with different porosity but having the same permeability. We suggest to use the shear rate noted $\dot{\gamma}$ which is however not a quantity directly available from measurements in complex geometries. The shear rate is critical for polymer systems flowing in porous media and an empirical law has been established by Chauveteau [19] in sandstones and bead-packs. Very recently Pedroni [20] have shown that this law can be successfully used for foam flow in homogeneous sandstones. From a classical rheological point of view the Chauveteau law can be expressed as follow:

$$\dot{\gamma} = 4\frac{v_i}{l_s}\alpha(K_w), \qquad (2)$$

with v_i the interstitial velocity, l_s the typical length scale of the sheared zone and α an empirical correction which is a decreasing function of the water permeability K_w. The length l_s is the pore throat estimated from conduit flow model as $\sqrt{8K_w/\phi}$. Extrapolating from Chauveteau et al. data [19], we found $\alpha \simeq 3.7275$ for 225 mD and $\alpha \simeq 2.189$ for 1550 mD. Plotting the foam apparent viscosity against the shear rate calculated with the above coefficients yields a unique curve (Figure 8). Thus the data obtained from different permeability and porosity are reduced to a single power law curve with exponent close to -1 (between -0.90 and -0.95)

The water saturation (also plotted on Figure 8) increases monotonously, from 10 to 20%, as the foam relative viscosity decreases with the shear rate. As η_r^f decreases the foam becomes less effective in reducing the CO_2 flow and the gas may flow more easily along the preferential paths, resulting in an increase of the water saturation. Furthermore one could also observe that water saturation is always below the injected water fraction $f_w = 1 - f_g = 30\%$. It means that the gas mobility is well reduced within the rock and the generated foam is very efficient for the whole range of interstitial velocity used here: from 3 ft/day to 100 ft/day, representative range from in depth fluid velocities to near wellbore.

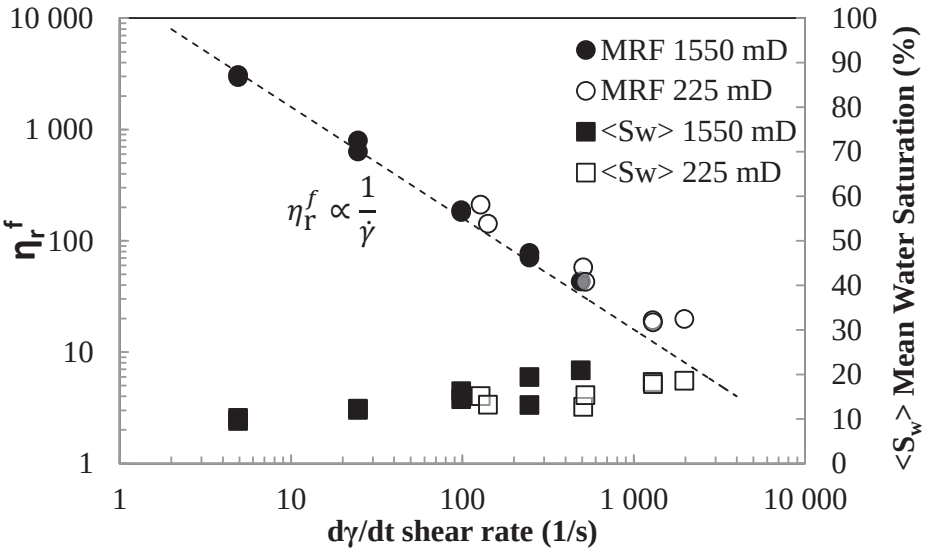

Figure 8: The foam relative viscosity η_r^f (circles) and the mean water saturation <S_w> (squares) vs. the shear rate $\dot{\gamma}$ computed from eq. (2) in Clashach sandstone at 30°C and a pore pressure of 10 bar. The full symbols represent data for a 1550 mD sandstone with a porosity about 20%. The empty symbols for 225 mD with a porosity about 12%. The dotted line corresponds to the equation $\eta_r^f = 16000/\dot{\gamma}$.

Performing the same analysis for the high pressure data, the shear rate $\dot{\gamma}$ was estimated from eq. (2) with $\alpha = 2.605$ for $K_w = 820$ mD and $\phi = 20.0$ %. We observed that the foam relative viscosity η_r^f can be described with the same power law for both low and high pressure measurements (Figure 9). The exponents are respectively -0.94 and -0.92 for the low and high pressure conditions. Thus, at steady state, the generated CO_2-foam shows the same ability to reduce the gas flow, whatever the pressure.

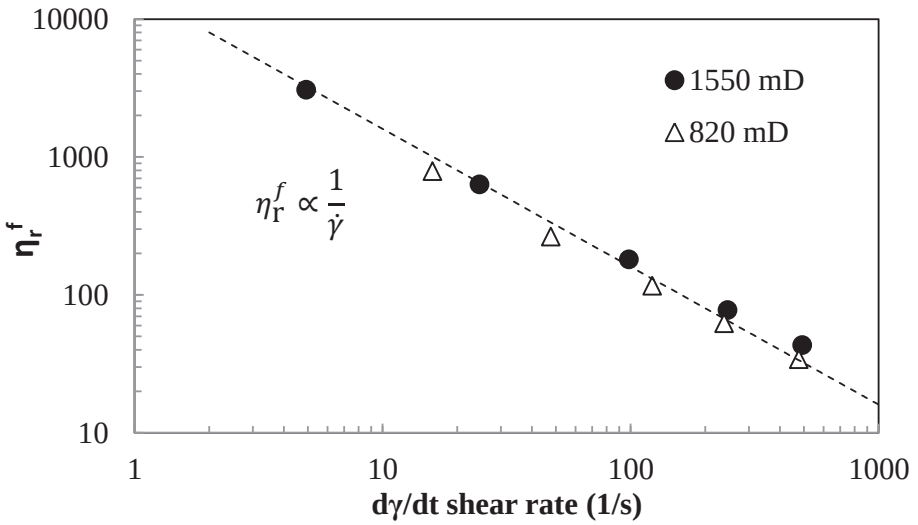

Figure 9: Comparison between low (full circle - 1550 mD) and high pressure (empty triangles - 820 mD) experiments for the decreasing velocities (as in reservoir application). The shear rate is computed from eq. (2). The dotted line is the same power law as plotted on Fig. 8 : $\eta_r^f = 16000/\dot{\gamma}$.

6. Conclusion

We studied the performance of CO_2 foams as a mean to reduce the gas flow rate in the vicinity of fractures or reactivated faults in the context of CO_2 storage. The laboratory experiments were conducted on typical sandstones representative of storage formations, with permeabilities in the range 200-1500 mD, and porosities between 10 and 20 %. The surfactant-brine solution and the CO_2 were co-injected at the inlet face of the sample using two different set-ups, in which the local saturation profiles are measured either by magnetic resonance imaging or by X-ray attenuation. These set-ups allowed observing the onset of foam as a function of interstitial velocity, in the largest possible range from about 3 ft/day up to 100 ft/day. The performance of the generated foams was evaluated from the relative foam viscosity, the ratio of the measured pressure drop in the presence of foam to the pressure drop in single phase condition for the same interstitial velocity. Whatever the pressure and permeability/porosity, the relative foam viscosity can be described as a power law vs. the shear rate evaluated from an empirical law established for polymer systems in which the interstitial velocity, permeability and porosity are the main variables. The exponent is close to -1 describing the shear-thinning behavior.

Acknowledgements

We acknowledge Solvay for providing the surfactant used in this study. Research in this paper was conducted with funding from the European Commission FP7 project MiReCOl, Grant Agreement n° 608608. The project received additional funding from Statoil, ENGIE and Shell.

References

[1] MIT Energy Initiative Symposium, Role of Enhanced Oil Recovery in Accelerating the Deployment of Carbon Capture and Sequestration (2010).
[2] S. Thomas, Enhanced Oil Recovery - An Overview, Oil & Gas Science and Technology - Rev. IFP 63 (2008) 9–19.
[3] K. Damen, A. Faaij, W. Turkenburg, Health, Safety and Environmental Risks of Underground Co2 Storage – Overview of Mechanisms and Current Knowledge, Climatic Change 74 (2006) 289–318.
[4] P. A. Gauglitz, F. Friedmann, S. I. Kam, W. R. Rossen, Foam generation in homogeneous porous media, Chemical Engineering Science 57 (2002) 4037–4052.
[5] Dickson Tanzil, George J. Hirasaki, Clarence A. Miller, Conditions for Foam Generation in Homogeneous Porous Media (2002) SPE 75176.
[6] A.R. Kovscek, Patzek T. W., C.J. Radke, Mechanistic Prediction of Foam Displacement in Multidimensions: A Population Balance Approach (1994) SPE/DOE 27789.
[7] G. Batôt, M. Fleury, Rosenberg E., L. Nabzar, M. Chabert, Foam Propagation in Rock Samples: Impact of Oil and Flow Caracterization, SPE EOR OGWA Oman SPE-179855-MS (2016).
[8] Z. I. Khatib, G. J. Hirasaki, A. H. Falls, Effects of Capillary Pressure on Coalescence and Phase Mobilities in Foams Flowing Through Porous Media, SPE Reservoir Engineering (1988) 919–926.
[9] R.M. Enick, Olsen D. K., Mobility and Conformance Control for Carbon Dioxyde Enhanced Oil Recovery (CO2-EOR) via Thickeners, Foams, and Gels - A detailed Literature Review of 40 years of Research, DOE/NETL-2012/1540 (2012).
[10] W.R. Brock, L.A. Bryan, Summary Results of CO2 EOR Field Tests, 1972-1987 (1989).
[11] A. Skauge, M.G. Aarra, L. Surguchev, H.A. Martinsen, L. Rasmussen, Foam-Assisted WAG: Experience from the Snorre Field (2002) SPE 75157.
[12] W.J. McLendon, P. Koronaios, R.M. Enick, G. Biesmans, L. Salazar, A. Miller, Y. Soong, T. McLendon, V. Romanov, D. Crandall, Assessment of CO2-soluble non-ionic surfactants for mobility reduction using mobility measurements and CT imaging, Journal of Petroleum Science and Engineering 119 (2014) 196–209.

[13] Bernard G.G., Holm L.W., Method for recovering oil from subterranean formations US patent 3 342 256 (1967).
[14] W.T. Osterloh and M.J. Jante Jr., Effects of Gas and Liquid Velocity on Steady-State Foam Flow at High Temperature (1992) SPE/DOE 24179.
[15] J.M. Alvarez, H.J. Rivas, and W.R. Rossen, Unified Model for Steady-State Foam Behavior at High and Low Foam Qualities, SPE journal (2001) SPE 74141.
[16] K. Ma, J.L. Lopez-Salinas, M.C. Puerto, C.A. Miller, S.L. Biswal, G.J. Hirasaki, Estimation of Parameters for the Simulation of Foam Flow through Porous Media. Part 1: The Dry-Out Effect, Energy Fuels 27 (2013) 2363–2375.
[17] A. Moradi-Araghi, E.L. Johnston, D.R. Zornes, K.J. Harpole, Laboratory Evaluation of Surfactants for CO2-Foam Applications at the South Cowden Unit (1997) SPE 37218.
[18] Chabert M., Morvan M., L. Nabzar, Advanced screening technologies for the selection of dense CO2 foaming surfactants (2012) SPE 154147.
[19] G. Chauveteau, A. Zaitoun, Basic rheological behavior of xanthan polysaccharide solutions in porous media: effects of pore size and polymer concentration Developments in Petroleum Science 13, Enhanced Oil Recovery: Proceedings of the Third European Symposium on Enhanced Oil Recovery (1981) 197–212.
[20] L. Pedroni, Private communications.